iScience

CellPress
OPEN ACCESS

Article

Reaction and separation system for CO_2 hydrogenation to formic acid catalyzed by iridium immobilized on solid phosphines under base-free condition

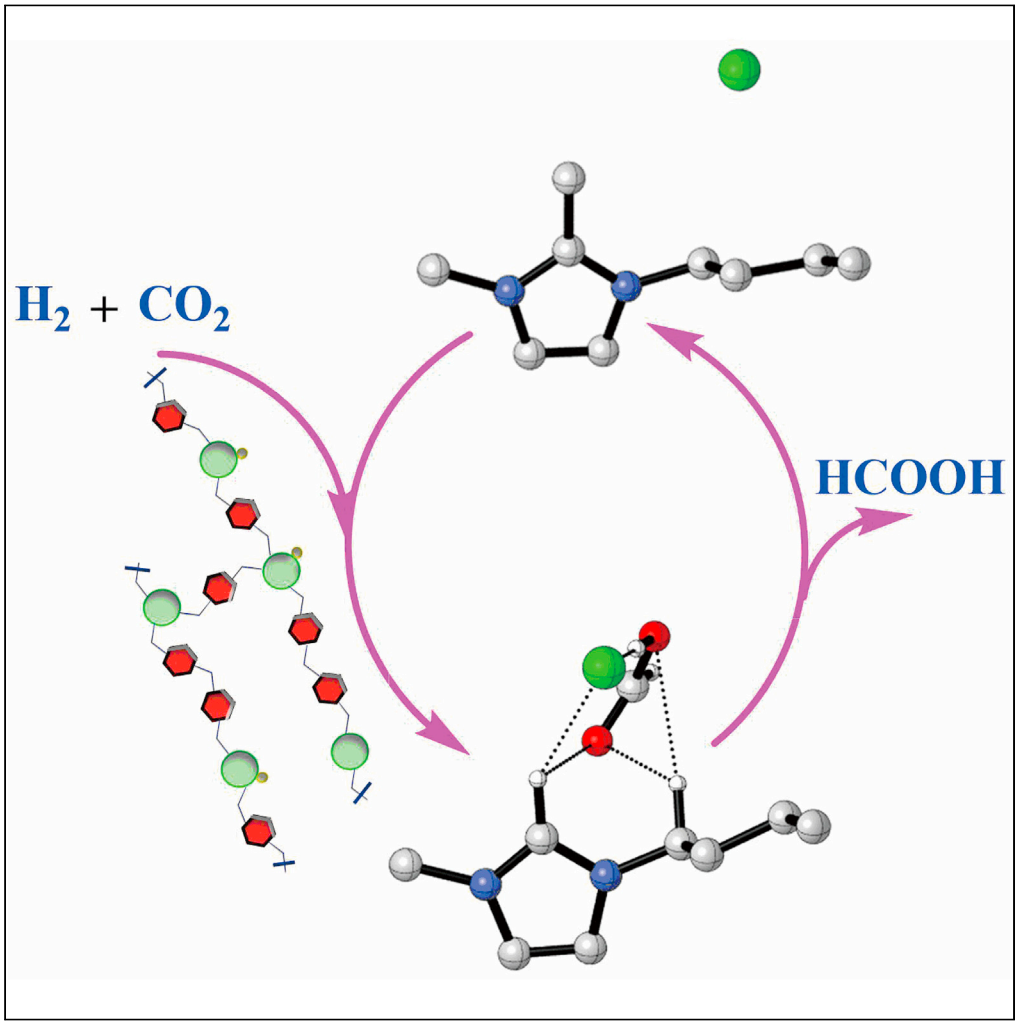

Jinling Hu, Wentao Ma, Qiang Liu, Jiao Geng, Youting Wu, Xingbang Hu

gengjiao@nju.edu.cn (J.G.)
huxb@nju.edu.cn (X.H.)

Highlights

An effective catalyst that can catalyze CO_2 hydrogenation to formic acid under base-free condition

An immobilized catalyst that is much inert in HCOOH decomposition than the homogeneous one

Effective HCOOH separation from the catalytic system

Catalyst and solvent can be recycled

Hu et al., iScience 26, 106672
May 19, 2023
https://doi.org/10.1016/j.isci.2023.106672

iScience

CellPress
OPEN ACCESS

Article

Reaction and separation system for CO_2 hydrogenation to formic acid catalyzed by iridium immobilized on solid phosphines under base-free condition

Jinling Hu,[1,2] Wentao Ma,[1,2] Qiang Liu,[1] Jiao Geng,[1,*] Youting Wu,[1] and Xingbang Hu[1,3,*]

SUMMARY

Hydrogenation of carbon dioxide (CO_2) to produce formic acid (HCOOH) in base-free condition can avoid waste producing and simplify product separation process. However, it remains a big challenge because of the unfavorable energy in both thermodynamics and dynamics. Herein, we report the selective and efficient hydrogenation of CO_2 to HCOOH under neutral conditions with imidazolium chloride ionic liquid as the solvent, catalyzed by a heterogeneous Ir/PPh_3 compound. The heterogeneous catalyst is more effective than the homogeneous one because it is inert in catalyzing the decomposition of product. A turnover number (TON) of 12700 can be achieved, and HCOOH with a purity of 99.5% can be isolated by distillation because of the non-volatility of the solvent. Both the catalyst and imidazolium chloride can be recycled at least 5 times with stable reactivity.

INTRODUCTION

Carbon dioxide (CO_2) is one of the major greenhouse gases.[1] The fractional concentration of CO_2 in the atmosphere has exceeded 400 ppm,[2,3] raising concern about climate change. Effective artificial CO_2 fixation becomes urgent.[4,5]

The use of CO_2 and hydrogen as feedstock to synthesize HCOOH is attractive. On the one hand, the hydrogenation of CO_2 to HCOOH is an ideal way with 100% theoretical atomic economy. On the other hand, HCOOH is currently considered as a promising candidate for hydrogen storage. Hydrogenation of CO_2 requires simultaneous activation of both CO_2 and H_2, which is quite difficult because of the kinetic and thermodynamic stability of CO_2 and H_2.[6–9] Some transition metal-based complexes have been reported that can activate both H_2 and CO_2, such as Ru,[7,8,10–18] Ir,[19–26] Pd,[27–30] Au,[31–33] Fe,[34–38] Mn,[39,40] Co,[41,42] Ni,[43–46] and Cu.[47–50]

However, the hydrogenation of CO_2 to HCOOH is thermodynamically unfavored (ΔG_{298K} = +33 kJ/mol).[6–9] To overcome thermodynamic limitations, these systems[49–51] require the use of bases and consequently produce stable formates.[6–10,13,15–50] As shown in Figure 1., these systems have extremely high catalytic activity, but acidification of the formate with strong acid produces waste salt.[52,53] To simplify the subsequent formic acid separation process, some studies on catalytic CO_2 hydrogenation in base-free systems have also been reported. Solutions containing DMSO[11,54,55] or acetate buffers[14,56,57] are typical examples. When DMSO was used, TON up to 4200 can be obtained. To further improve the TON, acetate buffer was adopted.[14,56,57]

On the other hand, most of the hydrogenation of CO_2 to HCOOH is catalyzed by homogeneous catalysts.[6–54] The existence of catalyst in the solution may be troublesome during formic acid separation because HCOOH or formate is not stable in the presence of these catalysts.[58–60] To develop an efficient and economical process for the hydrogenation of CO_2 to HCOOH, in addition to the neutral media, a heterogeneous catalyst with high catalytic activity is also crucial.

Figure 1 summarizes the current status of the hydrogenation of CO_2 to HCOOH or formate. Regarding the separation of HCOOH, an early paper described the use of amine exchange to separate the adduct of formic acid and triethylamine, which involved multi-step distillation.[61] Han et al. proposed a process in which

[1]School of Chemistry and Chemical Engineering, Nanjing University, 163 Xianlin Road, Qixia District, Nanjing 210023, P. R. China

[2]These author contributed equally

[3]Lead contact

*Correspondence: gengjiao@nju.edu.cn (J.G.), huxb@nju.edu.cn (X.H.)

https://doi.org/10.1016/j.isci.2023.106672

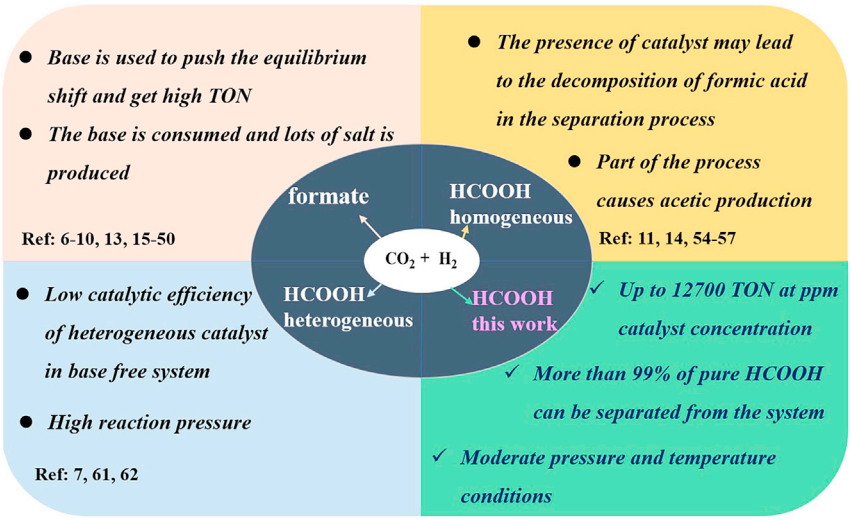

Figure 1. Catalytic CO_2 hydrogenation to HCOOH with diverse catalysts and stabilizing reagents

an immobilized ruthenium catalyst was used in water with an ionic liquid (IL) containing a tertiary amino group as the recyclable base.[62] Leitner et al. utilized the good solubility of HCOOH in supercritical CO_2 ($scCO_2$) and proposed a continuous flow hydrogenation of $scCO_2$ with integrated product separation from the immobilized catalyst and stabilized base to produce pure HCOOH in a single unit. An immobilized ruthenium organometallic catalyst and [pmmim][OOCH] were combined with supercritical CO_2 to achieve the highest TON 1938. However, only 14% HCOOH can be extracted in 74 h under at a pressure of 20 MPa.[7] These efforts combine well with hydrogenation of CO_2 and formic acid separation, but the efficiency of these catalysts is low compared to homogeneous catalysts.[14,55–57] Furthermore, the reaction conditions used in these systems are too harsh.

Herein, we developed an effective reaction and separation system for the hydrogenation of CO_2 to HCOOH catalyzed by a heterogeneous iridium compound under base-free condition. It includes the following key points: (1) A solution system forms multiple hydrogen-bonding with HCOOH which can facilitate the thermodynamic process of CO_2 hydrogenation to HCOOH; (2) easy separation of HCOOH because of the non-volatility of the solvent; (3) an effective heterogeneous catalyst avoids the HCOOH decomposition during the separation of HCOOH and exhibits higher reactivity than the homogeneous one in the hydrogenation of CO_2 to HCOOH.

RESULTS AND DISCUSSIONS

Catalyst synthesis and characterization

Homogeneous Iridium catalyst has high catalytic activity in the hydrogenation of CO_2 to HCOOH.[19–26] It would be more promising if it could be heterogeneous and reusable. Knitting aromatic polymers (KAPs) are good candidates to virtually transform highly active homogeneous catalysts into heterogeneous ones.[63] Grown by subsequent C−H activations of aromatic monomers, iridium complexes containing benzene rings can be heterogenized by self-polymerization without any prior functionalization. Previously, we have used this method to synthesize polymerized frustrated Lewis pairs.[64]

We first attempted to combine $[Ir(cod)Cl]_2$ with KAPs(Ph-PPh_3) to form KAPs(Ph-PPh_3)-Ir (Scheme S1). However, the reaction failed because Ir was barely detectable in the obtained compound. We then replaced part of PPh_3 in in the polymerization process with the complex $Ir(cod)Cl(PPh_3)$ [hereinafter referred to as Ir(I)-PPh_3] and KAPs(Ph-PPh_3-Ir) was obtained (Scheme 1). The growth of microporous network with Ir(I)-PPh_3 were confirmed by solid-state NMR, XPS spectroscopy, EDS elemental mapping analysis (Figure 2), FTIR spectroscopy (Figure S3). ^{13}C CP/MAS NMR of KAPs(Ph-PPh_3-Ir) (left part of Figure 2A) and KAPs(Ph-PPh_3) (left part of Figure 2B) are similar, with resonance peaks near 137 and 130 ppm corresponding to the substituted aromatic carbon and non-substituted aromatic carbon.[65] The resonance peak near 35.5 ppm indicates the existence of the methylene linker formed by Friedel–Crafts reaction. In the

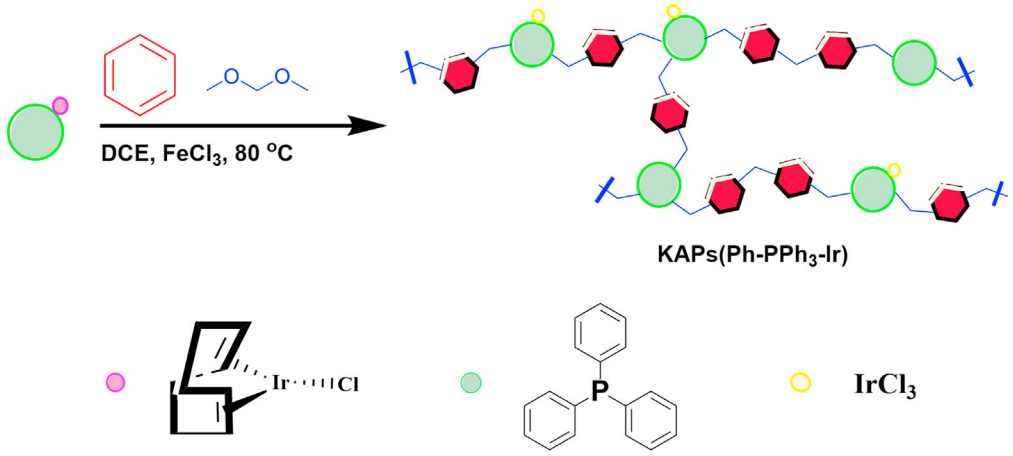

Scheme 1. Synthesis of KAPs(Ph-PPh_3-Ir)

^{31}P CP/MAS NMR spectra, a new peak appears at −24 ppm for KAPs(Ph-PPh_3-Ir), which is attributed to the Ir-coordinated P atoms. The P atoms involved in coordination are the majority (right part of Figure 2A). XPS study of KAPs(Ph-PPh_3-Ir) reveals he presence of C, P, Cl, and Ir elements in the solid material (Figure S6). The XPS pattern in Figure 2 shows that the Ir species in the KAPs(Ph-PPh_3-Ir) is in +3 oxidation state.[66] The oxidation state change may be because of the presence of $FeCl_3$ during the synthesis of KAPs(Ph-PPh_3-Ir), which acted as the catalyst in Friedel-Crafts reaction. To verify whether $FeCl_3$ can oxidize Ir(I) to Ir(III), we added $FeCl_3$ to the ether solution of Ir(I)-PPh_3. A white solid was rapidly precipitated from the solution. XPS pattern of the white solid shows that its binding energy is almost the same as that of Ir(III)-PPh_3. Although the binding energy of the polymerized iridium is different from that of Ir(III)-PPh_3, it is still within the range of Ir(III) reported in the literature (Ir $4f_{7/2}$: 62.6 ev–62.7 ev).[66] The atomic occupancy of each element in KAPs(Ph-PPh_3-Ir) is consistent with $Ir(PPh_3)_3Cl_3$. Figure 2E shows that Iridium is uniformly dispersed on the catalyst surface. The porous properties of the samples were analyzed by nitrogen adsorption analysis. The pore size distribution and the N_2 adsorption-desorption measurements of the catalyst were shown in Figures 2F and 2G. The BET surface area of KAPs(Ph-PPh_3-Ir) was 190.95 m^2/g. Thermogravimetric analysis (TGA) confirmed that the catalyst was very stable below 150 °C (see Figure S5).

CO_2 hydrogenation and HCOOH separation

The catalytic hydrogenation reactions of CO_2 to HCOOH were carried out using KAPs(Ph-PPh_3-Ir) as the catalyst. The KAPs(Ph-PPh_3) was used as the catalyst for control experiment and has no catalytic activity (entry 1, Table 1). Catalyzed by KAPs(Ph-PPh_3-Ir), DBU was almost completely converted to DBU formate with a TON of 159304 (entry 2, Table 1). In terms of catalytic hydrogenation of CO_2 to formate, the activity of KAPs (Ph-Ph_3-Ir) is much higher compared to the polymeric phenanthroline-Ir compound (TON: 40000).[67]

Because the hydrogenation of CO_2 to HCOOH is thermodynamically unfavored (ΔG_{298K} = +33 kJ/mol) in the absence of base,[6–9] we infer that the formation of multiple hydrogen bond between HCOOH and the solvent may compensate the Gibbs energy and shift the reaction toward the producing of HCOOH (Figure 3, Table S1, Figure S7). The energy released during hydrogen bond formation is rather weaker than that of the reaction between base and HCOOH, and therefore the energy consumption required for subsequent HCOOH separation can be greatly reduced. The hydrogenation of CO_2 to HCOOH in solvent can be divided into 3 steps (Scheme 2, Equations 1, 2, and 3). The overall reaction is presented in Equation 4. Thermodynamic calculations are performed based on the Equation 4 and the corresponding Gibbs free energy ($\Delta_r G$) and enthalpy ($\Delta_r H$) changes of reactions are listed in Table 1. For solvents containing inert C-H bond without hydrogen bond acceptor, the $\Delta_r G$ values are even larger than 33 kJ/mol (entries 3–5 in Table 1), indicating that the formation of HCOOH is further inhibited in these solvents. As a result, no HCOOH was produced in the hydrogenation experiments using n-hexane, benzene, or toluene as solvent. Although acetone, H_2O, and THF contain hydrogen bond acceptor, they are unable to promote the hydrogenation of CO_2 (entries 6–8 in Table 1). The cartesian coordinates of optimized structures were seen in Table S3.

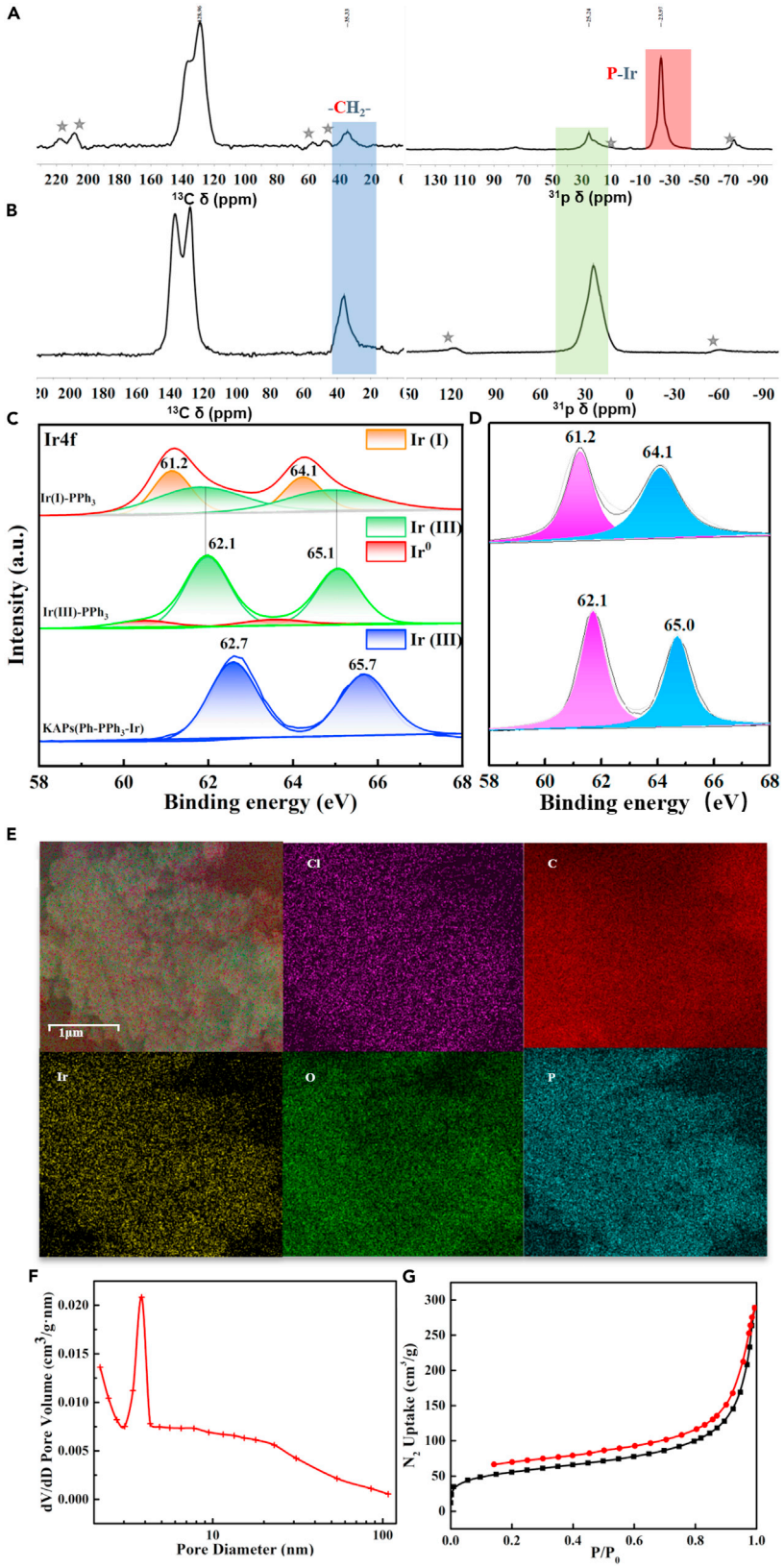
A
-CH2-
P-Ir
220 200 180 160 140 120 100 80 60 40 20 0
130 110 90 70 50 30 10 -10 -30 -50 -70 -90
13C δ (ppm)
31p δ (ppm)
B
20 200 180 160 140 120 100 80 60 40 20 0
150 120 90 60 30 0 -30 -60 -90
13C δ (ppm)
31p δ (ppm)
C
Ir4f
Ir (I)
Ir (III)
Ir0
61.2
64.1
Ir(I)-PPh3
62.1
65.1
Ir(III)-PPh3
62.7
65.7
KAPs(Ph-PPh3-Ir)
Intensity (a.u.)
58 60 62 64 66 68
Binding energy (eV)
D
61.2
64.1
62.1
65.0
58 60 62 64 66 68
Binding energy (eV)
E
1μm
Cl
C
Ir
O
P
F
dV/dD Pore Volume (cm3/g·nm)
0.020
0.015
0.010
0.005
0.000
10
100
Pore Diameter (nm)
G
N2 Uptake (cm3/g)
300
250
200
150
100
50
0
0.0 0.2 0.4 0.6 0.8 1.0
P/P0

Figure 2. Characterization of KAPs(Ph-PPh_3-Ir)

(A) Solid-state ^{31}C CP/MAS (left) and ^{31}P CP/MAS (right) spectra of KAPs(Ph-PPh_3-Ir).
(B) Solid-state ^{31}C CP/MAS (left) and ^{31}P CP/MAS (right) spectra of KAPs(Ph-PPh_3).
(C) XPS pattern for Ir of Ir(I)-PPh_3, $IrCl_3$/PPh_3 and KAPs(Ph-PPh_3-Ir).
(D) XPS pattern for Ir on Ir(I)-PPh_3 before (above) and after (below) it was treated with $FeCl_3$.
(E) EDS images of KAPs(Ph-PPh_3-Ir) with the corresponding element distribution maps as insets.
(F) The pore width distribution of KAPs(Ph-PPh_3-Ir).
(G) Nitrogen adsorption (black square) and desorption (red circle) isotherms of KAPs(Ph-PPh_3-Ir).

Ionic liquid consisting of cation and anion can be used as reaction solvent and provides both strong hydrogen bond donor and acceptor. When [emim][Cl],[bmim][Cl], and [hmim][Cl] are used as solvent, the $\Delta_r G$ values are only 10.58–15.49 kJ/mol (entries 11–13 in Table 1), indicating that these solvents can facilitate the formation of HCOOH. The hydrogenation of CO_2 in [hmim][Cl] gave a TON of 12700, which was much higher than those using neutral solvent. For example, the highest TON was 4200 when DMSO was used as solvent.[11,54,55] The $\Delta_r G$ values show that solution containing acetate buffer can significantly improve the stability of formic acid and this is consistent with literature reports.[14,56,57] When [emim][OAc] or [bmim][OAc] was used as solvent, the TON can reach 53832 (entries 14–15 in Table 1). However, owing to the stronger acidity of HCOOH, HCOOH can react with CH_3COO^- to produce $HCOO^-$ and CH_3COOH, which will bring more difficulty for the separation of HCOOH. For the separation of HCOOH-[bmim][OAc], the distillate obtained from the distillation experiment contained 86.3% CH_3COOH and only 13.7% HCOOH (Figure 4).

Table 1. Energy value and TON data of CO_2 hydrogenation to HCOOH catalyzed by KAPs(Ph-PPh_3-Ir) in different solvents

Entry	Solvent	ΔrH (kJ/mol)	ΔrG (kJ/mol)	TON[a]
1[b]	DBU (20 mmol)	−90.94	−18.99	0
2	DBU (20 mmol)	−90.94	−18.99	159304
3	n-hexane (2 mL)	−4.75	63.82	<1
4	benzene (2 mL)	−15.49	49.52	<1
5	toluene (2 mL)	−18.29	44.67	<1
6	acetone (2 mL)	−38.51	30.85	<1
7	Water (2 mL)	−37.83	30.66	<1
8	THF (2 mL)	−47.27	29.76	<1
9	[emim][BF_4] (10 mmol)	−37.53	29.84	92
10	[emim][Br] (10 mmol)	−49.41	26.84	150
11	[emim][Cl] (10 mmol)	−55.29	13.99	9550
12	[bmim][Cl] (10 mmol)	−49.46	15.49	11800
13	[hmim][Cl] (10 mmol)	−46.63	10.58	12700
14	[emim][OAc] (10 mmol)	−84.64	−4.21	50000
15	[bmmim][OAc] (10 mmol)	−104.66	−8.08	53832
16	$N_{1888}Cl$ (10 mmol)	−54.65	23.26	1667
17	$NH_3 \cdot H_2O$ (20 mmol)	−56.03	10.45	23330
18[c]	[emim][Cl] (10 mmol)	−55.29	13.99	205
19[d]	[bmim][Cl] (10 mmol)	−49.46	15.49	1170
20[b]	[bmim][Cl] (10 mmol)	−49.46	15.49	0

[a]Standard conditions: KAPs(Ph-PPh_3-Ir) (5 mg, 0.12 μmol Ir based on ICP-OES); reaction temperature (100°C); CO_2 (3MPaat room temperature), H_2 (4MPaat room temperature); reaction time (21 h). TON: turnover numbers. TON= n(HCOOH determined by NMR)/n(Ir determined by ICP-OES). TONs are mean values from at least two independent experiments with a mean deviation of ±(5–10) %.
[b]5 mg KAPs(Ph-PPh_3) was used instead of KAPs(Ph-PPh_3-Ir).
[c]Catalyzed by Ir(I)-PPh_3 (0.001 mmol).
[d]Catalyzed by Ir(I)-PPh_3 (0.0001 mmol) and 5 mg KAPs(Ph-PPh_3).

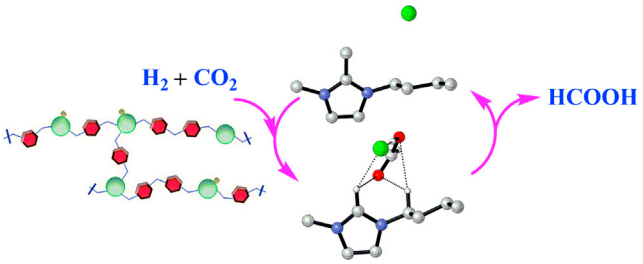

Figure 3. Promoting the CO_2 hydrogenation to HCOOH by KAPs(Ph-PPh_3-Ir) and multiple hydrogen bond

A simple separation process after reaction is vital for large scale industrial application. A further systematic investigation of the distillation of different CO_2 hydrogenation solutions was carried out. The ^1H NMR of the original solutions, residues and distillates are shown in Figure S9, and HCOOH concentrations in both distillate and bottom residue are presented in Figure 4. DBU and other strong organic or inorganic bases were widely used in the CO_2 hydrogenation.[6–10,13,15–50] DBU and HCOOH reacted rapidly to form formate [DBUH][HCOO], and no distillate can be obtained even when the temperature of vacuum distillation was raised to 150 °C. When DMSO was used as solvent-a case widely used to promote base-free CO_2 hydrogenation,[11,54,55] there was a large amount of solvent in the distillate and the concentration of HCOOH in the distillate was only 1.8% after the primary distillation. This is similar to the case of formic acid separated from imidazolium acetates. The boiling points of HCOOH and DMSO or acetic acid are close to each other. It is difficult to separate HCOOH and the solvent in one distillation, thus increasing the energy consumption for product separation. From the perspective of Product Lifecycle Management, excessive energy consumption in the separation process will obviously decrease the contribution of reaction process to the carbon neutralization.

Because [emim][Cl] has almost no vapor pressure, HCOOH could be easily separated without the loss of [emim][Cl]. More importantly, pure HCOOH can be obtained by primary distillation. Combining the literature data[7,62] and the several systems we have separated, imidazolium chloride system is more effective because HCOOH can be easily isolated from [emim][Cl] with a purity of 99.5% and only 0.1% HCOOH in the residue by vacuum distillation. It should be emphasized that HCOOH is stable in [emim][Cl] in the absence of a catalyst, even at temperatures up to 140 °C, and therefore losses because of the decomposition of formic acid during distillation can be neglected.

Catalytic effect evaluation

To better understand the inherent influencing factors of CO_2 hydrogenation reaction, the reaction temperature and the partial pressure of CO_2 and H_2 is expanded. Within a certain temperature range, the efficiency of catalytic CO_2 hydrogenation increased with increasing temperature. With further increase in temperature, the rate of formic acid decomposition accelerated, which inhibited the increase of TON (Table S2). The highest TON was obtained at 100 °C (Figure 5A). Moreover, the hydrogenation of CO_2 to HCOOH is an entropy-reducing process[8] and high temperatures are not favorable for product generation. Figure 5B confirms this. Although the highest TON was obtained at 100°C, it is recommended to perform the reaction at a lower temperature if higher concentrations of HCOOH are required. When the reaction was performed at 80 °C, the HCOOH concentration increased linearly (Figure 5B) because the HCOOH decomposition was almost negligible comparing with the CO_2 hydrogenation (entry 3, Table S2). The decomposition of formic acid significantly accelerated when the temperature rose to

$$H_2\,(g) + CO_2\,(g) \longrightarrow HCOOH\,(g) \quad (1)$$

$$HCOOH\,(g) \longrightarrow HCOOH\,(l) \quad (2)$$

$$HCOOH\,(l) + Solvent\,(l) \longrightarrow HCOOH \text{ --- } Solvent\,(l) \quad (3)$$

$$H_2\,(g) + CO_2\,(g) + Solvent\,(l) \longrightarrow HCOOH \text{ --- } Solvent\,(l) \quad (4)$$

Scheme 2. CO_2 hydrogenation process in solvent

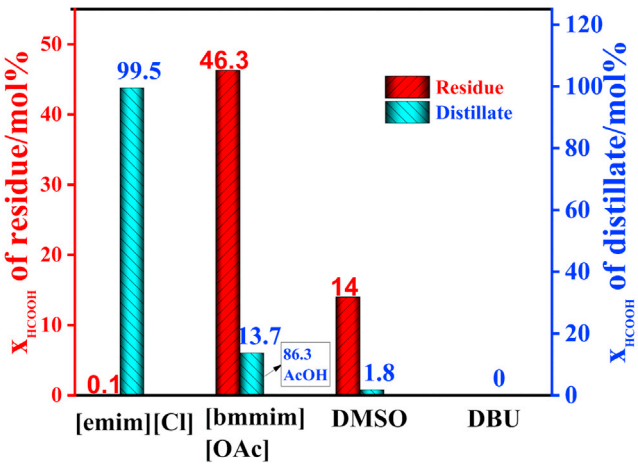

Figure 4. The HCOOH concentration in both distillate and residue of different systems after vacuum distillation

X_{HCOOH}= n(HCOOH determined by ^{1}H NMR)/n(Solvent determined by ^{1}H NMR).

100 °C and above (entry 4, Table S2). In fact, the catalyst was able to catalyze almost complete decomposition of HCOOH at this temperature and at ambient pressure (Figure S10). The equilibrium of this reaction will be reached more quickly with the increase of temperature under the same pressure conditions, and the concentration of formic acid at equilibrium is reduced (Figure 5B).

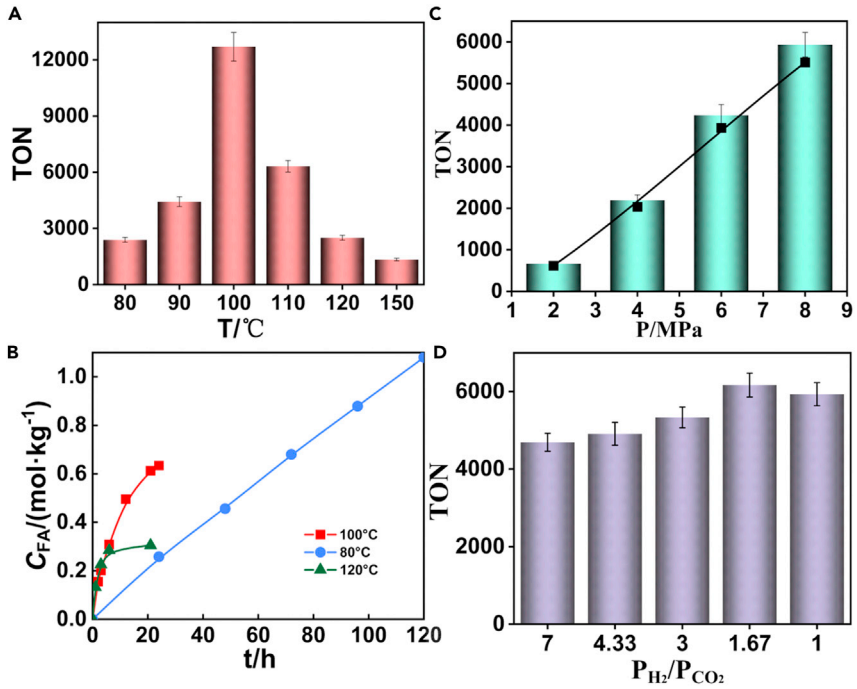

Figure 5. Effects of different reaction conditions on carbon dioxide hydrogenation efficiency

(A) Effect of temperature on TON. CO_2 (3MPaat room temperature), H_2 (4MPaat room temperature); reaction time (21 h). TON= n(HCOOH determined by NMR)/n(Ir determined by ICP-OES). TONs are mean values from at least two independent experiments with a mean deviation of ±(5–10) %.

(B) Concentration of HCOOH as a function of reaction time at the temperature of 80 °C (blue circle), 100 °C (green square and 120 °C (red triangle). CO_2 (3MPaat room temperature), H_2 (4MPaat room temperature). C_{FA}= n(HCOOH determined by NMR)/m(solvent added before hydrogenation).

(C) The influence of total pressure on the TON (P_{H2}/P_{CO2} = 1, 4h).

(D) The influence of the ratio of p_{H2} and p_{CO2} on TON (total pressure was 8 MPa, 4h).

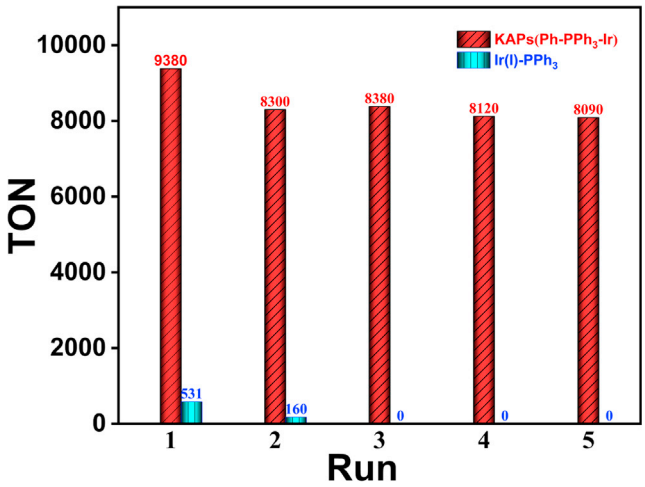

Figure 6. Recycling of catalyst and ionic liquid in the CO_2 hydrogenation

Conditions: KAPs(Ph-PPh_3-Ir) (4.5 mg, 0.1 μmol Ir based on ICP-OES); Ir(I)-PPh_3 (0.1 μmol); [emim][Cl] (10 mmol); reaction temperature (100 °C); CO_2 (3MPaat room temperature), H_2 (4MPaat room temperature); reaction time (21 h). TON= n(HCOOH determined by NMR)/n(Ir determined by ICP-OES). TONs are mean values from at least two independent experiments with a mean deviation of ±(5–10) %.

The effect of pressure was also investigated. A linear correlation in between TON and the total pressure can be observed (Figure 5C). The catalytic activity was also influenced by the ratio of P_{H2} and P_{CO2}, with the highest TON being obtained at a ratio of 1.67 (Figure 5D). Near the highest point, a drop in the partial pressure of CO_2 or H_2 led to a rapid decrease in TON.

Recycle of the catalyst and ionic liquid

In addition to TON and separation of HCOOH, an important aspect for the largescale industrial application is the robustness of catalysts and ionic liquid in recycling processes. The catalyst and ionic liquid were recycled and reused several times at 100 °C. Figure S11 shows the ^{1}H NMR of [emim][Cl] after each cycle, and no obvious structural changes are observed. The reaction activity of the catalyst presented a slight drop after the first cycle and it remained stable in the subsequent cyclic experiments. A TON of 8090 can be obtained after 5 recycle (Figure 6). To study changes of the catalytic species, further characterization of the recycled catalysts was performed. XPS pattern reveals that the oxidation state of Iridium changed after the first hydrogenation experiment, and remained unchanged in the subsequent cycles (Figure 7). To identify the coordination environment of the complex after reaction, attenuated total reflectance IR (ATR-IR) spectroscopy was performed. A new peak is detected at 2072 cm^{-1} for the recycled catalyst (Figure 7). The peak is most likely to be assigned as Ir-H (The IR spectrum shows absorptions at 2060–2112 cm^{-1}).[68,69] Based on these findings, it is proposed that the steep drop in activity after the first run is most likely caused by the changes in the coordination environment of catalytic center.[52]

To further understand the reactivity of the catalysts, the reusing of Ir(I)-PPh_3 was also carried out. Because the catalyst is homogeneous, it is remained in the solutions during the separation of HCOOH. The catalytic activity of Ir(I)-PPh_3 was completely lost after the second run (Figure 6). The ^{31}P NMR resonance split into two peaks after the catalyst was heated in [bmim] [Cl], which indicated Ir(I)-PPh_3 was unstable in the reaction process (Figure S12). We plotted the kinetic curves of HCOOH production from hydrogenation of carbon dioxide catalyzed by different iridium catalysts. The results show that oxidation of Ir(I) to Ir(III) improves the stability of the catalytic process, and monomer catalysts catalyzed the production of formic acid less effectively than heterogeneous catalysts (Figure S13). There may be two reasons. One is that the heterogeneous skeleton can successfully prevent Ir aggregation and precipitation, and the other is that the immobilization of the catalyst significantly reduces its efficiency in catalyzing the decomposition of formic acid (Table S2).

Conclusions

We have developed a highly effective reaction and separation system for CO_2 hydrogenation to HCOOH under base-free condition. A heterogeneous catalyst, KAPs(Ph-PPh_3-Ir), was combined with imidazolium

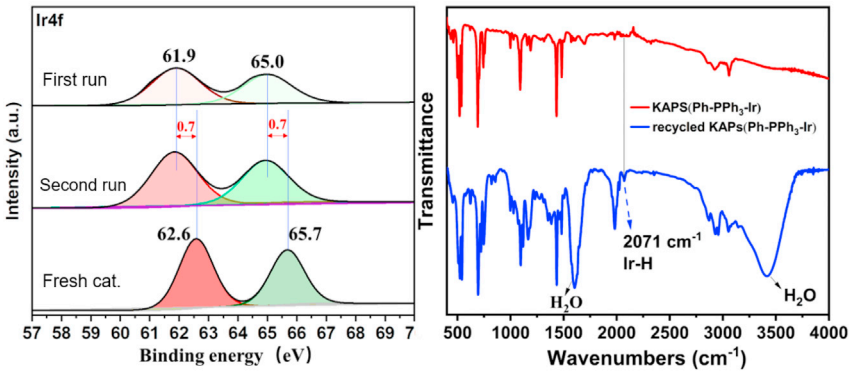

Figure 7. XPS patterns (left) and ATR-IR spectra (right) of the freshly prepared KAPs(Ph-PPh_3-Ir) and the KAPs(Ph PPh_3-Ir) after the CO_2 hydrogenation

chloride to exhibit high catalytic activity for the production of HCOOH. For the CO_2 hydrogenation, the polymerized catalyst is more reactive than the un-polymerized one because of its inertness in HCOOH decomposition. Catalytic turnovers as high as 12700 could be achieved. The highest HCOOH concentration was up to 1.09 mol/kg in [bmim][Cl]. HCOOH can be easily isolated with 99.5% purity and only 0.1% of HCOOH was remained in the residue by vacuum distillation. The catalyst and ionic liquid can be recycled and reused at least 5 cycles with satisfied efficiency. High TON, easy separation of HCOOH and catalyst, and high stability of the reaction system make the method reported here a potential pathway for producing HCOOH from CO_2 hydrogenation in industry.

Limitations of the study

This study reports a system for the direct catalytic hydrogenation of carbon dioxide to formic acid and its separation. However, this article only investigated the catalytic performance based on iridium/triphenylphosphine catalysts. Therefore, further studies are needed to investigate the catalytic performance of catalysts based on other metal complexes and to improve the practical application prospects of carbon dioxide hydrogenation to formic acid.

STAR★METHODS

Detailed methods are provided in the online version of this paper and include the following:

- KEY RESOURCES TABLE
- RESOURCE AVAILABILITY
  - Lead contact
  - Materials availability
  - Data and code availability
- METHOD DETAILS
  - General reagent information
  - General analytical information
  - Synthesis of IrCl(cod)(PPh_3) [Ir(I)-PPh_3 was used in the text to refer to this compound]
  - Synthesis of synthesis of KAPs(Ph-PPh_3) and KAPs(Ph-PPh_3-Ir)
  - Synthesis of synthesis of Ir(III)-PPh_3
  - Calculations of the interaction between solvent molecules and formic acid
  - Catalytic hydrogenation of CO_2 to formic acid
  - Separation HCOOH from the solution
  - Stability testing of formic acid
  - Experiments on the decomposition of formic acid catalyzed by different catalysts
  - Hydrogenation of CO_2 to formic acid catalyzed by different catalysts

SUPPLEMENTAL INFORMATION

Supplemental information can be found online at https://doi.org/10.1016/j.isci.2023.106672.

ACKNOWLEDGMENTS

This work was supported by National Natural Science Foundation of China (No. 22178159 and 21878141).

AUTHOR CONTRIBUTIONS

Conceptualization, J.H., J.G., and X.H.; methodology, J.H., W.M., Q.L., and X.H.; investigation, J.H., W.M., and Q.L.; writing – original draft, J.H., J.G., and X.H.; writing – original draft, J.G., Y.W., and X.H.; supervision, J.G., Y.W., and X.H.; funding acquisition, X.H.

DECLARATION OF INTERESTS

The authors declare no competing interests.

Received: November 28, 2022
Revised: February 14, 2023
Accepted: April 10, 2023
Published: April 22, 2023

REFERENCES

1. Zhao, Y., Wang, T., Wang, Y., Hao, R., and Hui, W. (2020). Simultaneous absorption and hydrogenation of CO_2 from flue gas by KBH(4)catalyzed by nickel nanoparticles supported on TiO_2. Chem. Eng. J. *380*, 122523. https://doi.org/10.1016/j.cej.2019.122523.

2. Tollefson, J. (2009). Growing agricultural benefits for climate. Nature *462*, 966–967.

3. Kang, D.H., Jo, W.G., Yun, Y.S., Yu, H.S., Jang, S.W., Kim, D.L., Park, J.H., Song, Y.C., and Choi, Y.J. (2020). Research for carbon dioxide fluctuation using drone above the mud flat and reed beds in the suncheon bay. J. Environ. Sci. Int. *29*, 703–713. https://doi.org/10.5322/jesi.2020.29.7.703.

4. Xingyuan, G., Shangkun, D., and Sibudjing, K. (2022). Zeolite-based catalytic membrane reactors for thermo-catalytic conversion of CO_2. iScience *25*, 105343. https://doi.org/10.1016/j.isci.2022.105343.

5. Peng, L., Jurca, B., Primo, A., Gordillo, A., Parvulescu, V.I., and García, H. (2022). High C2-C4 selectivity in CO_2 hydrogenation by particle size control of Co-Fe alloy nanoparticles wrapped on N-doped graphitic carbon. iScience *25*, 104252. https://doi.org/10.1016/j.isci.2022.104252.

6. Leitner, W., Dinjus, E., and Gaßner, F. (1994). Activation of carbon-dioxide .4. rhodium-catalyzes hydrogenation of carbon-dioxide to formic-acid. J. Organomet. Chem. *475*, 257–266. https://doi.org/10.1016/0022-328x(94)84030-x.

7. Wesselbaum, S., Hintermair, U., and Leitner, W. (2012). Continuous-flow hydrogenation of carbon dioxide to pure formic acid using an integrated $scCO_2$ process with immobilized catalyst and base. Angew. Chem. Int. Ed. *51*, 8585–8588. https://doi.org/10.1002/anie.201203185.

8. Schaub, T., and Paciello, R.A. (2011). A process for the synthesis of formic acid by CO_2 hydrogenation: thermodynamic aspects and the role of CO. Angew. Chem. Int. Ed. *50*, 7278–7282. https://doi.org/10.1002/anie.201101292.

9. Wang, W.-H., Himeda, Y., Muckerman, J.T., Manbeck, G.F., and Fujita, E. (2015). CO_2 hydrogenation to formate and methanol as an alternative to photo- and electrochemical CO_2 reduction. Chem. Rev. *115*, 12936–12973. https://doi.org/10.1021/acs.chemrev.5b00197.

10. Huff, C.A., and Sanford, M.S. (2013). Catalytic CO_2 hydrogenation to formate by a ruthenium pincer complex. ACS Catal. *3*, 2412–2416. https://doi.org/10.1021/cs400609u.

11. Moret, S., Dyson, P.J., and Laurenczy, G. (2014). Direct synthesis of formic acid from carbon dioxide by hydrogenation in acidic media. Nat. Commun. *5*, 4017. https://doi.org/10.1038/ncomms5017.

12. Bontemps, S., Vendier, L., and Sabo-Etienne, S. (2012). Borane-Mediated carbon dioxide reduction at ruthenium: formation of C1 and C2 compounds. Angew. Chem. Int. Ed. *51*, 1671–1674. https://doi.org/10.1002/anie.201107352.

13. Kuriki, R., Sekizawa, K., Ishitani, O., and Maeda, K. (2015). Visible-light-driven CO_2 reduction with carbon nitride: enhancing the activity of ruthenium catalysts. Angew. Chem. Int. Ed. *54*, 2406–2409. https://doi.org/10.1002/anie.201411170.

14. Weilhard, A., Qadir, M.I., Sans, V., and Dupont, J. (2018). Selective CO_2 hydrogenation to formic acid with multifunctional ionic liquids. ACS Catal. *8*, 1628–1634. https://doi.org/10.1021/acscatal.7b03931.

15. Li, Z., Rayder, T.M., Luo, L., Byers, J.A., and Tsung, C.-K. (2018). Aperture-opening encapsulation of a transition metal catalyst in a metal-organic framework for CO_2 hydrogenation. J. Am. Chem. Soc. *140*, 8082–8085. https://doi.org/10.1021/jacs.8b04047.

16. Estes, D.P., Leutzsch, M., Schubert, L., Bordet, A., and Leitner, W. (2020). Effect of ligand electronics on the reversible catalytic hydrogenation of CO_2 to formic acid using ruthenium polyhydride complexes: a thermodynamic and kinetic study. ACS Catal. *10*, 2990–2998. https://doi.org/10.1021/acscatal.0c00404.

17. Ahn, S., Park, K., Lee, K.R., Haider, A., Nguyen, C.V., Jin, H., Yoo, S.J., Yoon, S., and Jung, K.-D. (2022). Atomically dispersed Ru(III) on N-doped mesoporous carbon hollow spheres as catalysts for CO_2 hydrogenation to formate. Chem. Eng. J. *442*, 136185. https://doi.org/10.1016/j.cej.2022.136185.

18. Jaleel, A., Haider, A., Nguyen, C.V., Lee, K.R., Choung, S., Han, J.W., Baek, S.-H., Shin, C.-H., and Jung, K.-D. (2022). Structural effect of Nitrogen/Carbon on the stability of anchored Ru catalysts for CO(2) hydrogenation to formate. Chem. Eng. J. *433*, 133571. https://doi.org/10.1016/j.cej.2021.133571.

19. Tanaka, R., Yamashita, M., and Nozaki, K. (2009). Catalytic hydrogenation of carbon dioxide using Ir(III)-Pincer complexes. J. Am. Chem. Soc. *131*, 14168–14169. https://doi.org/10.1021/ja903574e.

20. Schmeier, T.J., Dobereiner, G.E., Crabtree, R.H., and Hazari, N. (2011). Secondary coordination sphere interactions facilitate the insertion step in an iridium(III) CO_2 reduction catalyst. J. Am. Chem. Soc. *133*, 9274–9277. https://doi.org/10.1021/ja2035514.

21. Hull, J.F., Himeda, Y., Wang, W.-H., Hashiguchi, B., Periana, R., Szalda, D.J., Muckerman, J.T., and Fujita, E. (2012). Reversible hydrogen storage using CO_2 and a proton-switchable iridium catalyst in aqueous media under mild temperatures and pressures. Nat. Chem. *4*, 383–388. https://doi.org/10.1038/nchem.1295.

22. Liu, C., Xie, J.-H., Tian, G.-L., Li, W., and Zhou, Q.-L. (2015). Highly efficient hydrogenation of carbon dioxide to formate catalyzed by iridium(III) complexes of imine-diphosphine ligands. Chem. Sci. *6*, 2928–2931. https://doi.org/10.1039/c5sc00248f.

23. Kanega, R., Onishi, N., Szalda, D.J., Ertem, M.Z., Muckerman, J.T., Fujita, E., and Himeda, Y. (2017). CO2 hydrogenation catalysts with deprotonated picolinamide ligands. ACS Catal. *7*, 6426–6429. https://doi.org/10.1021/acscatal.7b02280.

24. An, B., Zeng, L., Jia, M., Li, Z., Lin, Z., Song, Y., Zhou, Y., Cheng, J., Wang, C., and Lin, W. (2017). Molecular iridium complexes in metal-organic frameworks catalyze CO_2 hydrogenation via concerted proton and hydride transfer. J. Am. Chem. Soc. *139*, 17747–17750. https://doi.org/10.1021/jacs.7b10922.

25. Shao, X., Yang, X., Xu, J., Liu, S., Miao, S., Liu, X., Su, X., Duan, H., Huang, Y., and Zhang, T. (2019). Iridium single-atom catalyst performing a quasi-homogeneous hydrogenation transformation of CO2 to formate. Chem *5*, 693–705. https://doi.org/10.1016/j.chempr.2018.12.014.

26. Gunasekar, G.H., Park, K., Ganesan, V., Lee, K., Kim, N.-K., Jung, K.-D., and Yoon, S. (2017). A covalent triazine framework, functionalized with Ir/N-heterocyclic carbene sites, for the efficient hydrogenation of CO_2 to formate. Chem. Mater. *29*, 6740–6748. https://doi.org/10.1021/acs.chemmater.7b01539.

27. Bi, Q.-Y., Lin, J.-D., Liu, Y.-M., Du, X.-L., Wang, J.-Q., He, H.-Y., and Cao, Y. (2014). An aqueous rechargeable formate-based hydrogen battery driven by heterogeneous Pd catalysis. Angew. Chem. Int. Ed. *53*, 13583–13587. https://doi.org/10.1002/anie.201409500.

28. Su, J., Yang, L., Lu, M., and Lin, H. (2015). Highly efficient hydrogen storage system based on ammonium bicarbonate/formate redox equilibrium over palladium nanocatalysts. ChemSusChem *8*, 813–816. https://doi.org/10.1002/cssc.201403251.

29. Mori, K., Sano, T., Kobayashi, H., and Yamashita, H. (2018). Surface engineering of a supported PdAg catalyst for hydrogenation of CO2 to formic acid: elucidating the active Pd atoms in alloy nanoparticles. J. Am. Chem. Soc. *140*, 8902–8909. https://doi.org/10.1021/jacs.8b04852.

30. Kuwahara, Y., Fujie, Y., Mihogi, T., and Yamashita, H. (2020). Hollow mesoporous organosilica spheres encapsulating PdAg nanoparticles and poly(ethyleneimine) as reusable catalysts for CO_2 hydrogenation to formate. ACS Catal. *10*, 6356–6366. https://doi.org/10.1021/acscatal.0c01505.

31. Preti, D., Squarcialupi, S., and Fachinetti, G. (2012). Conversion of syngas into formic acid. ChemCatChem *4*, 469–471. https://doi.org/10.1002/cctc.201200046.

32. Filonenko, G.A., Vrijburg, W.L., Hensen, E.J., and Pidko, E.A. (2016). On the activity of supported Au catalysts in the liquid phase hydrogenation of CO_2 to formates. J. Catal. *343*, 97–105. https://doi.org/10.1016/j.jcat.2015.10.002.

33. Liu, Q., Yang, X., Li, L., Miao, S., Li, Y., Li, Y., Wang, X., Huang, Y., and Zhang, T. (2017). Direct catalytic hydrogenation of CO_2 to formate over a Schiff-base-mediated gold nanocatalyst. Nat. Commun. *8*, 1407. https://doi.org/10.1038/s41467-017-01673-3.

34. Federsel, C., Boddien, A., Jackstell, R., Jennerjahn, R., Dyson, P.J., Scopelliti, R., Laurenczy, G., and Beller, M. (2010). A well-defined iron catalyst for the reduction of bicarbonates and carbon dioxide to formates, alkyl formates, and formamides. Angew. Chem. Int. Ed. *49*, 9777–9780. https://doi.org/10.1002/anie.201004263.

35. Zhang, Y., MacIntosh, A.D., Wong, J.L., Bielinski, E.A., Williard, P.G., Mercado, B.Q., Hazari, N., and Bernskoetter, W.H. (2015). Iron catalyzed CO_2 hydrogenation to formate enhanced by Lewis acid co-catalysts. Chem. Sci. *6*, 4291–4299. https://doi.org/10.1039/c5sc01467k.

36. Langer, R., Diskin-Posner, Y., Leitus, G., Shimon, L.J.W., Ben-David, Y., and Milstein, D. (2011). Low-pressure hydrogenation of carbon dioxide catalyzed by an iron pincer complex exhibiting noble metal activity. Angew. Chem. Int. Ed. *50*, 9948–9952. https://doi.org/10.1002/anie.201104542.

37. Ziebart, C., Federsel, C., Anbarasan, P., Jackstell, R., Baumann, W., Spannenberg, A., and Beller, M. (2012). Well-defined iron catalyst for improved hydrogenation of carbon dioxide and bicarbonate. J. Am. Chem. Soc. *134*, 20701–20704. https://doi.org/10.1021/ja307924a.

38. Coufourier, S., Gaignard Gaillard, Q., Lohier, J.-F., Poater, A., Gaillard, S., and Renaud, J.-L. (2020). Hydrogenation of CO_2, hydrogenocarbonate, and carbonate to formate in water using phosphine free bifunctional iron complexes. ACS Catal. *10*, 2108–2116. https://doi.org/10.1021/acscatal.9b04340.

39. Dubey, A., Nencini, L., Fayzullin, R.R., Nervi, C., and Khusnutdinova, J.R. (2017). Bio-inspired Mn(I) complexes for the hydrogenation of CO_2 to formate and formamide. ACS Catal. *7*, 3864–3868. https://doi.org/10.1021/acscatal.7b00943.

40. Sun, Q., Chen, B.W.J., Wang, N., He, Q., Chang, A., Yang, C.-M., Asakura, H., Tanaka, T., Hülsey, M.J., Wang, C.-H., et al. (2020). Zeolite-encaged Pd-Mn nanocatalysts for CO(2)Hydrogenation and formic acid dehydrogenation. Angew. Chem. Int. Ed. *59*, 20183–20191. https://doi.org/10.1002/anie.202008962.

41. Jeletic, M.S., Mock, M.T., Appel, A.M., and Linehan, J.C. (2013). A cobalt-based catalyst for the hydrogenation of CO_2 under ambient conditions. J. Am. Chem. Soc. *135*, 11533–11536. https://doi.org/10.1021/ja406601v.

42. Burgess, S.A., Appel, A.M., Linehan, J.C., and Wiedner, E.S. (2017). Changing the mechanism for CO_2 hydrogenation using solvent-dependent thermodynamics. Angew. Chem. Int. Ed. *56*, 15002–15005. https://doi.org/10.1002/anie.201709319.

43. Burgess, S.A., Kendall, A.J., Tyler, D.R., Linehan, J.C., and Appel, A.M. (2017). Hydrogenation of CO_2 in water using a bis(diphosphine) Ni-H complex. ACS Catal. *7*, 3089–3096. https://doi.org/10.1021/acscatal.7b00350.

44. Vogt, C., Groeneveld, E., Kamsma, G., Nachtegaal, M., Lu, L., Kiely, C.J., Berben, P.H., Meirer, F., and Weckhuysen, B.M. (2018). Unravelling structure sensitivity in CO_2 hydrogenation over nickel. Nat. Catal. *1*, 127–134. https://doi.org/10.1038/s41929-017-0016-y.

45. Cammarota, R.C., Vollmer, M.V., Xie, J., Ye, J., Linehan, J.C., Burgess, S.A., Appel, A.M., Gagliardi, L., and Lu, C.C. (2017). A bimetallic nickel-gallium complex catalyzes CO_2 hydrogenation via the intermediacy of an anionic d(10) nickel hydride. J. Am. Chem. Soc. *139*, 14244–14250. https://doi.org/10.1021/jacs.7b07911.

46. Zhao, Y., Wang, T., Wang, X., Hao, R., and Wang, H. (2018). CO_2 hydrogenation to formate over nano-scale zero-valent nickel catalyst under atmospheric pressure. Chem. Eng. J. *347*, 860–869. https://doi.org/10.1016/j.cej.2018.04.079.

47. Zall, C.M., Linehan, J.C., and Appel, A.M. (2015). A molecular copper catalyst for hydrogenation of CO_2 to formate. ACS Catal. *5*, 5301–5305. https://doi.org/10.1021/acscatal.5b01646.

48. Zall, C.M., Linehan, J.C., and Appel, A.M. (2016). Triphosphine-ligated copper hydrides for CO_2 hydrogenation: structure, reactivity, and thermodynamic studies. J. Am. Chem. Soc. *138*, 9968–9977. https://doi.org/10.1021/jacs.6b05349.

49. Romero, E.A., Zhao, T., Nakano, R., Hu, X., Wu, Y., Jazzar, R., and Bertrand, G. (2018). Tandem copper hydride-Lewis pair catalysed reduction of carbon dioxide into formate with dihydrogen. Nat. Catal. *1*, 743–747. https://doi.org/10.1038/s41929-018-0140-3.

50. Hu, J., Liu, J., Yao, C., Zhou, L., Wu, Y., Zhang, Z., and Hu, X. (2021). Effective hydrogenation of CO_2 to formate catalyzed by ionic liquid modified acetate-Cu. Green Chem. *23*, 951–956. https://doi.org/10.1039/d0gc03502e.

51. Zhao, T., Hu, X., Wu, Y., and Zhang, Z. (2019). Hydrogenation of CO_2 to formate with H-2: transition metal free catalyst based on a Lewis pair. Angew. Chem. Int. Ed. *58*, 722–726. https://doi.org/10.1002/anie.201809634.

52. Zhang, J.Z., Li, Z., Wang, H., and Wang, C.Y. (1996). Homogeneous catalytic synthesis of formic acid (salts) by hydrogenation of CO_2 with H_2 in the presence of ruthenium species. J. Mol. Catal. Chem. *112*, 9–14. https://doi.org/10.1016/1381-1169(96)00185-9.

53. Leitner, W. (1995). Carbon-dioxide as a raw-materia-the syntheis of formic-acid and its derivatives from CO_2. Angew. Chem. Int. Ed. *34*, 2207–2221. https://doi.org/10.1002/anie.199522071.

54. Jens, C.M., Scott, M., Liebergesell, B., Westhues, C.G., Schäfer, P., Franciò, G., Leonhard, K., Leitner, W., and Bardow, A. (2019). Rh-catalyzed hydrogenation of CO_2 to formic acid in DMSO-based reaction media: solved and unsolved challenges for process

development. Adv. Synth. Catal. *361*, 307–316. https://doi.org/10.1002/adsc.201801098.

55. Rohmann, K., Kothe, J., Haenel, M.W., Englert, U., Hölscher, M., and Leitner, W. (2016). Hydrogenation of CO_2 to formic acid with a highly active ruthenium acriphos complex in DMSO and DMSO/water. Angew. Chem. Int. Ed. *55*, 8966–8969. https://doi.org/10.1002/anie.201603878.

56. Weilhard, A., Argent, S.P., and Sans, V. (2021). Efficient carbon dioxide hydrogenation to formic acid with buffering ionic liquids. Nat. Commun. *12*, 231. https://doi.org/10.1038/s41467-020-20291-0.

57. Weilhard, A., Salzmann, K., Navarro, M., Dupont, J., Albrecht, M., and Sans, V. (2020). Catalyst design for highly efficient carbon dioxide hydrogenation to formic acid under buffering conditions. J. Catal. *385*, 1–9. https://doi.org/10.1016/j.jcat.2020.02.027.

58. Zell, T., and Milstein, D. (2015). Hydrogenation and dehydrogenation iron pincer catalysts capable of metal ligand cooperation by aromatization/dearomatization. Acc. Chem. Res. *48*, 1979–1994. https://doi.org/10.1021/acs.accounts.5b00027.

59. Bertini, F., Mellone, I., Ienco, A., Peruzzini, M., and Gonsalvi, L. (2015). Iron(II) complexes of the linear rac-tetraphos-1 ligand as efficient homogeneous catalysts for sodium bicarbonate hydrogenation and formic acid dehydrogenation. ACS Catal. *5*, 1254–1265. https://doi.org/10.1021/cs501998t.

60. Bielinski, E.A., Lagaditis, P.O., Zhang, Y., Mercado, B.Q., Würtele, C., Bernskoetter, W.H., Hazari, N., and Schneider, S. (2014). Lewis acid-assisted formic acid dehydrogenation using a pincer-supported iron catalyst. J. Am. Chem. Soc. *136*, 10234–10237. https://doi.org/10.1021/ja505241x.

61. Preti, D., Resta, C., Squarcialupi, S., and Fachinetti, G. (2011). Carbon dioxide hydrogenation to formic acid by using a heterogeneous gold catalyst. Angew. Chem. Int. Ed. *50*, 12551–12554. https://doi.org/10.1002/anie.201105481.

62. Zhang, Z., Xie, Y., Li, W., Hu, S., Song, J., Jiang, T., and Han, B. (2008). Hydrogenation of carbon dioxide is promoted by a task-specific ionic liquid. Angew. Chem. Int. Ed. *47*, 1127–1129. https://doi.org/10.1002/anie.200704487.

63. Valverde-Gonzalez, A., Iglesias, M., and Maya, E.M. (2021). Metal catalysis with knitting aryl polymers: design, catalytic applications, and future trends. Chem. Mater. *33*, 6616–6639. https://doi.org/10.1021/acs.chemmater.1c01569.

64. Liu, Q., Yang, L., Yao, C., Geng, J., Wu, Y., and Hu, X. (2021). Controlling the Lewis acidity and polymerizing effectively prevent frustrated Lewis pairs from deactivation in the hydrogenation of terminal alkynes. Org. Lett. *23*, 3685–3690. https://doi.org/10.1021/acs.orglett.1c01073.

65. Li, B., Guan, Z., Wang, W., Yang, X., Hu, J., Tan, B., and Li, T. (2012). Highly dispersed Pd catalyst locked in knitting aryl network polymers for suzuki-miyaura coupling reactions of aryl chlorides in aqueous media. Adv. Mater. *24*, 3390–3395. https://doi.org/10.1002/adma.201200804.

66. Leigh, G.J., and Bremser, W. (1972). X-ray photoelectron spectroscopic studies of tertiary phosphine complexes of heavy transition-metals. J. Chem. Soc. Dalton Trans. 1216–1219. https://doi.org/10.1039/dt9720001216.

67. Gunasekar, G.H., and Yoon, S. (2019). A phenanthroline-based porous organic polymer for the iridium-catalyzed hydrogenation of carbon dioxide to formate. J. Mater. Chem. A. *7*, 14019–14026. https://doi.org/10.1039/c9ta03807h.

68. Barbaro, P., Bianchini, C., Meli, A., Peruzzini, M., Vacca, A., and Vizza, F. (1991). Assembling ethylene, alkyl, hydride, and CO ligands at iridium. Organometallics *10*, 2227–2238. https://doi.org/10.1021/om00053a028.

69. Zhou, L., Yao, C., Ma, W., Hu, J., Wu, Y., Zhang, Z., and Hu, X. (2021). CO_2 hydrogenation to formate catalyzed by highly stable and recyclable carbene-iridium under mild condition. J. CO2 Util. *54*, 101769. https://doi.org/10.1016/j.jcou.2021.101769.

70. Lebel, H., and Ladjel, C. (2008). Iridium complexes in olefination reactions. Organometallics *27*, 2676–2678. https://doi.org/10.1021/om800255c.

71. Orosz, K., Papp, G., Kathó, Á., Joó, F., and Horváth, H. (2019). Strong solvent effects on catalytic transfer hydrogenation of ketones with Ir(cod)(NHC)(PR3) catalysts in 2-propanol-water mixtures. Catalysts *10*, 17. https://doi.org/10.3390/catal10010017.

72. Chiu, Y.-C., Lin, C.-H., Hung, J.-Y., Chi, Y., Cheng, Y.-M., Wang, K.-W., Chung, M.-W., Lee, G.-H., and Chou, P.-T. (2009). Authentic-blue phosphorescent iridium(III) complexes bearing both hydride and benzyl diphenylphosphine; control of the emission efficiency by ligand coordination geometry. Inorg. Chem. *48*, 8164–8172. https://doi.org/10.1021/ic900607s.

73. Frisch, M.J., Trucks, G.W., Schlegel, H.B., Scuseria, G.E., Robb, M.A., Cheeseman, J.R., Scalmani, G., Barone, V., Mennucci, B., Petersson, G.A., et al. (2013). GAUSSIAN 09 (Revision E.01) (Gaussion, Inc.).

STAR★METHODS

KEY RESOURCES TABLE

REAGENT or RESOURCE	SOURCE	IDENTIFIER
Chemicals, peptides, and recombinant proteins		
Chloro(1,5-cyclooctadiene)iridium(I) dimer, ≥95%, RG	Adamas	Cat#17354D
Triphenylphosphine, 99%, RG	Adamas	Cat#69212E
Tetrahydrofuran	Honeywell	Cat#178810-1L
1,8-Diazabicyclo[5.4.0]undec-7-ene, 98%	MERYER	Cat#M33021-100G
n-hexane	Nanjing Reagent	Cat#C0760512205
Benzene	Nanjing Reagent	Cat#C0430010223
Toluene	Nanjing Reagent	Cat#C0430114023
Acetone	Nanjing Reagent	Cat#C0720114023
[emim][BF_4], 97%	MERYER	Cat#M83072-100G
[emim][Br], 98%	MERYER	Cat#M22808 -500G
[emim][Cl], 98%	MERYER	Cat#M83163 -500G
[bmim][Cl], 98%	MERYER	Cat#M26986 -500G
[hmim][Cl], 98%	MERYER	Cat#M72651-500G
[emim][OAc], 98%	MERYER	Cat#M83249-25G
N_{1888}Cl, 98%	DB	Cat#Q105271-500g
$NH_3 \cdot H_2O$	Honeywell	Cat#338818-1L
Iron(III) chloride, 98%	Adamas Chemical	Cat#82296A
Iridium(III) chloride, 99.9%	Adamas	Cat#10105K
Software and algorithms		
Origin 2022b	Origin Lab	https://www.originlab.com/
MestReNova	mestrelab	https://mestrelab.com/
Avantage	Thermo Fisher Scientific	https://www.thermofisher.cn/
Gaussian 09	Gaussian, Inc.	https://Gaussian.com/

RESOURCE AVAILABILITY

Lead contact

- Further information and requests for resources and reagents should be directed to the lead contact, Xingbang Hu (huxb@nju.edu.cn).

Materials availability

- No new materials were generated in this study, and all reagents were commercially available and used without purification.

Data and code availability

- The materials generated in this study will be made available on request.
- This paper does not report original code.
- Any additional information required to reanalyze the data reported in this paper is available from the lead contact upon request.

METHOD DETAILS

General reagent information

Commercially available reagents and chemicals were purchased and used without further purification.

H_2 (99.999 vt.%) and CO_2 (99.99 vt.%) were purchased from Nanjing Tianze Gas Center, Nanjing. Other reagents used in this article are listed in the key resources table.

General analytical information

NMR spectra were recorded on a Bruker AV 400 spectrometer. Ir element content analysis was conducted on agilent ICP-OES730. Fourier transform infrared spectroscopy (FT-IR) spectra were collected using a Bruker Tenson-27 FT-IR spectrometer. Solid-state nuclear magnetic resonance measurements were carried out using a Bruker AVIII NMR spectrometer (400 MHz) MHz). Scanning electron microscopy (SEM) and energy dispersive X-ray spectroscopy (EDS) elemental analysis were conducted by ZEISS GeminiSEM 300. Thermogravimetric analysis (TGA) was performed under N2 on a TGA Q 500, V20.13 with a balance gas flow of 10 mL/min and a sample gas flow of 25 mL/min. X-ray photoelectron spectroscopy (XPS) analysis was performed by PHI 5000 Versa Probe (ULVAC-PHI, JPN). Surface parameters were determined by using BET adsorption models, and pore size distributions were determined using the NLDFT model equipped in the instruments.

Synthesis of IrCl(cod)(PPh_3) [Ir(I)-PPh_3 was used in the text to refer to this compound]

0.43 g (0.64 mmmol) chloro-1,5-cyclooctadiene iridium dimer and 0.34 g (1.29 mmol) triphenylphosphine were added to 10 mL THF under a nitrogen atmosphere. The mixture was stirred at room temperature 20 min and then cooled to 0 °C and stirred 1 h.[70] The solvent was removed under reduced pressure and the pale brown powder was obtained. Yield: 0.53 g (69.3%). Ir(I)-PPh_3 was first reported by Lebel & Ladjel. Liquid NMR was used to characterize this compound (see Figure S1). And the spectra were consistent with those of similar structure reported in the literature.[71] XPS analysis was also carried out to detect the oxidation state of Ir (see Figure S2).

Synthesis of synthesis of KAPs(Ph-PPh_3) and KAPs(Ph-PPh_3-Ir)

$FeCl_3$ (anhydrous 9.75 g, 0.06 mol) was added to a solution of benzene (1.56 g, 0.02 mol), triphenylphosphine (5.25 g, 0.02 mol), and formaldehyde dimethyl acetal (FDA, 4.56 g, 0.06 mol) in 20 mL 1,2-dichloroethane (DCE). The resulting mixture was stirred at room temperature for good mixing, and then was stirred at 45 °C for 5 h to form original network. After that, it was heated at 80 °C for 67 h to react completely. The resulting precipitate was washed three times with methanol, then washed with methanol in a Soxhlet for 24 h, and finally dried under reduced pressure at 60 °C for 24 h. Yellowish brown solid (2.40 g) was obtained.[65] XPS and FT-IR were used to analysis the synthesized compound, which were well consistent with the ref.[65]

The synthesis of KAPs(Ph-PPh_3-Ir) referred to the synthesis steps of KAPs(Ph-PPh_3). $FeCl_3$ (anhydrous, 1.11 g) was added to a solution of benzene (0.18 g), Ir(I)-PPh_3 (0.6 g), PPh_3 (0.7 g) and formaldehyde dimethyl acetal (FDA, 0.52 g) in 2.5 mL 1,2-dichloroethane (DCE). The resulting mixture was stirred at 45 °C for 5 h to form original network. After that, it was heated at 80 °C for 96 h to react completely. The resulting precipitate was washed three times with methanol, then washed with methanol in a Soxhlet for 24 h, and finally dried under reduced pressure at 50 °C for 24 h. Pale yellow powder (0.49 g) was obtained.

Synthesis of synthesis of Ir(III)-PPh_3

A mix of $IrCl_3 \cdot 3H_2O$ (10 mg,0.028 mmol) and PPh_3 (36 mg, 0.14 mmol) in ethanol (2 mL) was refluxed for 12 h. Once removal of solvent in vacuum, the white powder was triturated with a 1:1 mixture of ester and solvent, and picked up by filtration (14 mg, 0.024 mmol, 85%).[72]

Calculations of the interaction between solvent molecules and formic acid

The calculations in this work were performed with the Gaussian09 software.[73] All the structures were optimized with M062X method. 6–311++G** basis set was used for all atoms. The IEF-PCM, SMD solvent model was used during the geometry optimizations to account for implicit solvent effects. The energy and force cut-offs: Maximum Force- 0 0.000012, RMS Force- 0.000002, Maximum Displacement- 0.0018, RMS Displacement- 0.0012. The cartesian coordinates of all structures are listed in the end of the supplemental

information. The implicit solvent model of isopropyl alcohol is used for ionic liquids because the dielectric constant of isopropyl alcohol is closer to that of ionic liquids.

Catalytic hydrogenation of CO_2 to formic acid

In a typical reaction, a 50 mL stainless autoclave was charged with KAPs(Ph-PPh_3-Ir) (5 mg) and 10 mmol [bmim][Cl]. The reactor was pressurized with 70 bar of an H_2: CO_2 (4:3) mixture, and the solution was stirred for 21hat 100 °C. Then, an aliquot of the reaction mixture was dissolved in 500 μL of $CDCl_3$ and the TON of the reaction was determined by ^{1}H NMR spectroscopy, using 1, 3, 5-trimethoxy benzene (1 mmol) as an internal standard (Figure S8).

Separation HCOOH from the solution

The HCOOH-solvent mixture was distilled at a pressure of 0.1 mbar. The distillation temperatures of each system were 110, 80, and 120 °C for HCOOH- [emim][Cl], HCOOH-DMSO, and HCOOH-[bmmim][OAc] respectively. The concentrations of HCOOH in the original solutions, the residues and the distillates were determined by ^{1}H NMR.

Stability testing of formic acid

The thermal stability of HCOOH in [emim][Cl] salt was tested with or without catalyst (Figure S10). HCOOH was added into [emim][Cl] to prepare 1M solution. Mixture A (without catalyst) was heated to 140 °C for 12 h. The concentration of HCOOH remained unchanged. Mixture B (with 5 mg KAPs(Ph-PPh_3-Ir)) was heated to 100 °C for 12 h. HCOOH was decomposed completely. Mixture C (with 5 mg KAPs(Ph-PPh_3-Ir)) was heated to 80 °C for 12 h. The content of HCOOH remained stable.

Experiments on the decomposition of formic acid catalyzed by different catalysts

The decomposition of formic acid was catalyzed by Ir(III)-PPh_3 and KAPs(Ph-PPh_3-Ir) at 80 and 100 °C, respectively. Formic acid and [emim][Cl] were added to a 25 mL flask with a concentration of 1M. Formic acid and ionic liquid were heated and mixed thoroughly. The concentration of HCOOH was accurately determined by ^{1}H NMR. Part of the solution was weighed and heated in an oil bath at 80 °C. 0.4 μmol Ir(III)-PPh_3 was added to the solution and the mixture wass stirred at 80 °C for 2 h. The sample was taken immediately after the reaction and cooled in an ice bath, and HCOOH concentration was analyzed by ^{1}H NMR. The temperature or catalyst was changed separately and the above steps were repeated to obtain other data.

Hydrogenation of CO_2 to formic acid catalyzed by different catalysts

Ir(I)-PPh_3, Ir(III)-PPh_3, KAPs(Ph-PPh_3-Ir) were used to catalyze the hydrogenation of CO_2 to formic acid. The amount of catalyst was 0.1 μmol. Other reaction conditions are the same as that in catalytic hydrogenation of CO_2 to formic acid. The reaction time of the experiment catalyzed by Ir(III)-PPh_3 doubled because equilibrium has not been reached in 21h.